

DOI:10.1002/ejic.201403160

Niobium-Containing Lindqvist Isopolyanions $[\text{Nb}_x\text{W}_{6-x}\text{O}_{19}]^{(2+x)-}$ Used as Precursors for Hydrodesulfurization Catalysts with Isomerization Properties

Karolina Bouadjadja-Rohan,^[a,b] Christine Lancelot,^[a]
Michel Fournier,^[a] Audrey Bonduelle-Skrzypczak,^[b]
Antoine Hugon,^[b] Olivier Mentré,^[a] and Carole Lamonier*^[a]

Keywords: Heterogeneous catalysis / Niobium / Tungsten / Isomerization / Lindqvist isopolyanion

Lindqvist isopolyanions $[\text{Nb}_x\text{W}_{6-x}\text{O}_{19}]^{(2+x)-}$ ($x = 0-4$ and 6) were prepared and their spectroscopic and thermal properties were determined by Raman and IR spectroscopy as well as TGA/DSC. The structure of the $[\text{NbW}_5\text{O}_{19}]^{3-}$ anion obtained as single crystal was determined. Ni-promoted alumina-supported hydrodesulfurization (HDS) catalysts were prepared from the best soluble NbW polyoxometalates. In the calcined catalysts, better dispersion of the metallic species is observed when using NbW isopolyanions instead of

the conventional ammonium metatungstate. The presence of niobium was expected to introduce acidity leading to isomerization property in classical NiW HDS catalysts. In HDS reaction conditions (under hydrogen pressure and sulfided environment) the cyclohexane isomerization into methylcyclopentane activity of niobium-based catalysts was found up to 5 times superior to that of conventional NiW catalyst, showing the beneficial effect of niobium for this reaction.

Introduction

Polyoxometalates (POMs) or polyanions are molecular metal oxides having different structures and proposing a combination of interesting chemical and physical properties. These materials can be largely applied in catalysis^[1-8] in the field of oxidation, isomerization or hydrodesulfurization reactions. Polyoxometalates constitute a family of mineral condensed ions in the form of isopolyanions and heteropolyanions. Isopolyanions $\text{M}_m\text{O}_y^{z-}$ (M is most frequently a metallic atom such as W and Mo) are formed during condensation of MO_4^{2-} oxoanions. This process takes place during acidification of starting solution with the elimination of water molecules and with creation of μ -oxo bonds between metal ions. In the presence of other XO_4^{2-} oxoanions (where X is different from M, being frequently a non-metallic atom such as B or Si), metallic atoms are associated around the second oxoanion and then, after polycondensation, an heteropolyanion is formed. Poly-

anions are represented by few families of compounds, among the major groups a few can be listed: Lindqvist $[\text{M}_x\text{M}'_{6-x}\text{O}_{19}]^{(2+x)-}$, Keggin $[\text{XM}_{12}\text{O}_{40}]^{n-}$, Anderson $[\text{XM}_6\text{O}_{24}\text{H}_6]^{n-}$ and Dawson $[\text{X}_2\text{M}_{18}\text{O}_{62}]^{n-}$, where M(M') is a metallic cation and X a non-metallic one. Niobium can form, among others, Lindqvist-type structure due to similar values of ionic radius of niobium(V) (0.64 Å) and tungsten(VI) (0.60 Å) in six-coordination according to ionic radii values reported by Shannon.^[9] Those elements can be combined in the frames of one structure forming $[\text{Nb}_x\text{W}_{6-x}\text{O}_{19}]^{(2+x)-}$ isopoly compounds.^[10] Figure 1 represents Lindqvist-type isopolyanion structure with six metallic atoms (depicted as large grey spheres) and 19 oxygen atoms (small spheres) which are divided into three subgroups: six terminal oxygen atoms bonded to only one met-

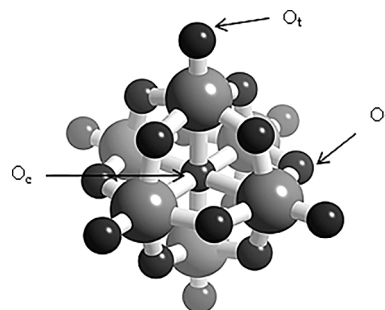


Figure 1. Lindqvist-type isopolyanion structure.^[19]

[a] Unité de Catalyse et Chimie du Solide, UCSC, UMR CNRS 8181, Université Lille Nord de France, 59655 Villeneuve d'Ascq, France
E-mail: carole.lamonier@univ-lille1.fr
ucsc.univ-lille1.fr
<http://ucsc.univ-lille1.fr/>

[b] IFP Energies Nouvelles, Rond-Point de l'Echangeur de Solaize, BP3, 69360 Solaize, France

Supporting information for this article is available on the WWW under <http://dx.doi.org/10.1002/ejic.201403160>.

allic atom (noted O_t), 12 atoms forming bridges (noted O_b) and one central oxygen atom being surrounded by six atoms of metal (noted O_c).^[11–14]

Hydrodesulfurization (HDS) of petroleum feedstocks for sulfur removal is a catalytic process generally performed with Ni(Co)W(Mo) alumina-supported catalysts, in which the active phase consists in well dispersed WS_2 (MoS₂) nanocrystallites decorated with Ni(Co) atoms. These active phases are obtained through the sulfidation of an oxidic precursor prepared by incipient wetness impregnation of alumina with an aqueous solution of ammonium metatungstate (ammonium heptamolybdate) and nickel nitrate (cobalt nitrate). Instead of these classical W(Mo) and Ni(Co) precursors, heteropolyanions (HPA) compounds containing Co and Mo or Ni and W atoms in the same entity were used as precursors of HDS catalysts; the corresponding enhancement of catalytic performance when compared with catalysts prepared from conventional precursors was attributed to better promotion due to the proximity of the active phase metals in the HPA entity.^[15–18]

In HDS of heavy fuels, acidity was identified as a factor accelerating hydrodesulfurization through for example isomerization of refractory sulfur-containing species.^[19–23] Niobium, due to its acidic character, might be particularly interesting in combination with tungsten for HDS catalysis. Niobium has been used as a dopant of HDS catalysts^[24–26] or as a support modifying agent.^[27] Due to the possibility to form niobium sulfide, it was also proposed as an independent hydrotreatment catalyst.^[28–30]

The aim of this work was to prepare niobium–tungsten-based Lindqvist isopolyanions as precursors for synthesizing hydrodesulfurization catalysts with acid properties: the initial proximity of Nb and W could lead to more efficient bifunctional catalysts thanks to an optimized distribution of both acid and HDS sites. A series of $[Nb_xW_{6-x}O_{19}]^{(2+x)-}$ anions was synthesized and characterized by Raman and Infrared spectroscopy. Thermogravimetric analysis was performed to determine the general formulas of the prepared compounds. The most soluble salts were selected to prepare alumina-supported NbW-Ni-promoted catalysts to assess their catalytic performance in isomerization of cyclohexane to methylcyclopentane.

Results and Discussion

Characterization of Isopolyanions

Vibrational Spectroscopy

There are only very few references dealing with the topic of NbW Lindqvist isopolyanions characterization by mean of vibrational spectroscopy. Rocchiccioli-Deltcheff et al.^[31] observed significant analogies between recorded Raman spectra for various NbW Lindqvist-type isopoly compounds and observed constant evolution towards the Raman spectrum of the last compound of the family $[Nb_6O_{19}]^{8-}$. Thus, they proposed the hypothesis that $[Nb_xW_{6-x}O_{19}]^{(2+x)-}$ anions possess hexatungstate structure

in which tungsten anions are progressively replaced by niobium.^[31]

The Figure 2 gathers the Raman spectra of the complete Lindqvist family $[Nb_xW_{6-x}O_{19}]^{(2+x)-}$, $x = 0, 1, 2, 3, 4, 6$ and allows to observe similarities in spectra shape from one compound to another as proposed by Rocchiccioli-Deltcheff et al.^[31] Raman high-frequency peaks (850–1000 cm^{-1}) are attributed to the metal-oxygen terminal vibrations for all oxygenated anions of elements of V A and VI A groups.^[32] In the Raman spectra of $[Nb_xW_{6-x}O_{19}]^{(2+x)-}$ HPAs, the evolution of the $Nb=O_t$ and $W=O_t$ band wavenumbers can be explained by the replacement of W par Nb that leads formally to symmetry lowering as for instance for $[NbW_5O_{19}]^{3-}$ with C_{4v} symmetry and $[Nb_2W_4O_{19}]^{4-}$ with C_{2v} symmetry. In this case, redistribution of potential energy of the anion leads to the partial mixture of $W=O_t$ and $Nb=O_t$ vibrators. In consequence, force constants of $Nb=O_t$ vibrators e.g. in $[Nb_3W_3O_{19}]^{5-}$ or $[Nb_4W_2O_{19}]^{6-}$ are expected to be displayed at higher wavenumber than for $[Nb_6O_{19}]^{8-}$ and correlatively force constants of $W=O_t$ vibrators are expected to be displayed at lower frequencies. Evolution of $W=O_t$ frequencies towards lower frequencies by increasing Nb content is clearly observed in Figure 2. For the $[W_6O_{19}]^{2-}$ isopolyanion TMA salt, $\nu_s W = O_t$ terminal vibration is displayed at 1001 cm^{-1} and shifts towards lower wavenumber when decreasing tungsten loading, reaching 929 cm^{-1} for $K_6[Nb_4W_2O_{19}]$. (Figure 2). Peak corresponding to the asymmetric tungsten–oxygen vibration $\nu_{as} W = O_t$ also shifts toward lower wavenumber when decreasing tungsten loading, with values of 977 cm^{-1} for $[W_6O_{19}]^{2-}$ and 937 cm^{-1} for $[Nb_3W_3O_{19}]^{5-}$ isopolyanions. Comparison of $[W_6O_{19}]^{2-}$ with $[Nb_6O_{19}]^{8-}$ Raman spectra shows $M=O_t$ vibrations frequencies higher for tungsten than for niobium which is in accordance with more ionic character of $Nb=O_t$. For $K_8[Nb_6O_{19}]$ isopolyanion $\nu_s Nb = O_t$ characteristic peak is observed at 883 cm^{-1} . This band is noted also for other Nb-containing isopolyanions, at 880 cm^{-1} for $[Nb_4W_2O_{19}]^{6-}$, around 893 cm^{-1} for $[Nb_3W_3O_{19}]^{5-}$ and at 914 cm^{-1} for $[NbW_5O_{19}]^{3-}$. This evol-

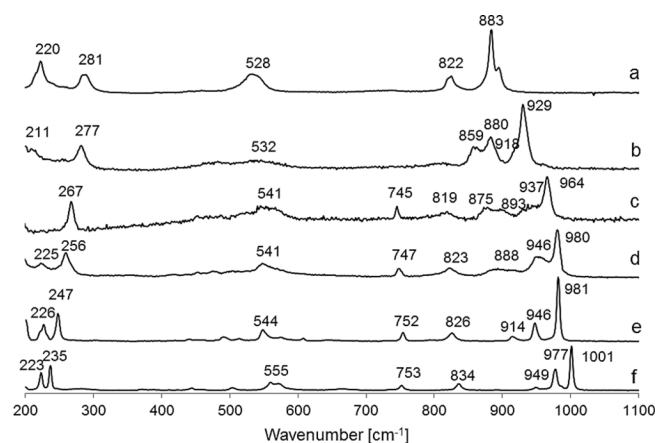


Figure 2. Raman spectra of $[Nb_xW_{6-x}O_{19}]^{(2+x)-}$ isopolyanions salts: (a) $[Nb_6O_{19}]^{8-}$ (b) $[Nb_4W_2O_{19}]^{6-}$ (c) $[Nb_3W_3O_{19}]^{5-}$ (d) $[Nb_2W_4O_{19}]^{4-}$ (e) $[NbW_5O_{19}]^{3-}$ (f) $[W_6O_{19}]^{2-}$.

ution is more difficult to point out for less intense Nb=O_t vibrations for which a tightening of ν_sNbO_t and ν_{as}NbO_t peaks can be observed. Indeed, regardless of the tungsten content in mixed isopolyanion NbW, ν_sW = O_t terminal vibration is the dominating one in agreement with stronger polarisability of W=O_t in comparison with Nb=O_t.

Peaks observed for all the compounds from about 800 cm⁻¹ to 400 cm⁻¹ correspond to νMO_b vibrations. Peaks displayed at low frequencies from 235 cm⁻¹ for [W₆O₁₉]²⁻ till 281 cm⁻¹ for [Nb₆O₁₉]⁸⁻ correspond to symmetric stretching ν_sMO_c. They are observed at 267 cm⁻¹ for [Nb₃W₃O₁₉]⁵⁻ and at 256 cm⁻¹ for [Nb₂W₄O₁₉]⁴⁻ and correspond to ν_sWO_c vibration. Furthermore, for TMA-containing salts, a peak at 946 cm⁻¹ is attributed to an asymmetric C–N stretching vibration^[33,34] and it can be observed on spectra c, d and e on Figure 2. For the TMA salt of [Nb₃W₃O₁₉]⁵⁻ this peak is incorporated into larger peak containing also ν_{as}WO_t vibration.

Infrared spectra (Figure 3) also display characteristic bands of metal–oxygen bonds^[32,35] also confirming successful formation of [Nb_xW_{6-x}O₁₉]^{(2+x)-} isopoly compounds. We observe characteristic bands of Infrared spectra (Figure 3) at 982 cm⁻¹ for [W₆O₁₉]²⁻ isopolyanion. This band shifts toward lower wavenumber with decreasing tungsten content till 958 cm⁻¹ for [NbW₅O₁₉]³⁻. Not all the W=O_t vibrations are easily observable due to weak coupling between W=O_t vibrators that are quite distant one from another^[32] Nb=O_t vibration band is observed at about 856 cm⁻¹ for [Nb₆O₁₉]⁸⁻ and moves toward higher wavenumber with decreasing niobium content.

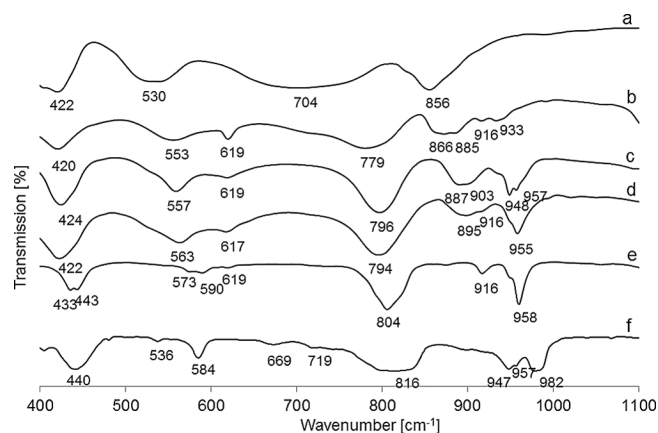


Figure 3. Infrared spectra of [Nb_xW_{6-x}O₁₉]^{(2+x)-} isopolyanions salts: (a) [Nb₆O₁₉]⁸⁻ (b) [Nb₄W₂O₁₉]⁶⁻ (c) [Nb₃W₃O₁₉]⁵⁻ (d) [Nb₂W₄O₁₉]⁴⁻ (e) [NbW₅O₁₉]³⁻ (f) [W₆O₁₉]²⁻.

As previously observed for Raman spectra, a decrease of W=O_t bands wavenumber and an increase of Nb=O_t frequencies with increasing tungsten loading (decreasing niobium content) can also be highlighted for IR spectra. A band corresponding to the presence of the cation is observed around 795 cm⁻¹ for compounds containing significant amounts of TMA. Bands at 700–810 cm⁻¹ and at 530–580 cm⁻¹ correspond to νMO_b vibrations and at 400–440 cm⁻¹ to νMO_c vibrations.

Single-Crystal and Powder X-ray Diffraction for [NbW₅O₁₉]³⁻ salt

Among four NbW synthesized isopolyanions, [NbW₅O₁₉]³⁻ salt was obtained as single crystal. Its crystallographic structure is formed of one independent Lindqvist HPA, two independent TMA molecules and one independent potassium countercations arranged within a cubic geometry [Space group 225 – International Tables for Crystallography – *Fm* $\bar{3}$ *m*, R1(*F*) for all reflexions: 2.14%]. In the anions, Nb and W are disordered over a 24(e) position and their relative occupancies are refined to Nb/W = 22(1)%:78(1)%. In the last cycles of refinement the ratio was fixed to the expected 16.6:83.3% without significant changes in the convergence process. If one considers the Lindqvist unit as a super-octahedron, each of its six external species is bounded to a K⁺ cations [K–O = 2.8557(7)], such that K⁺ is at the center of a KO₆ octahedron (Figure 4). Also eight TMA molecules surround each HPA with their C3 faces parallel to the faces of the super-octahedron.

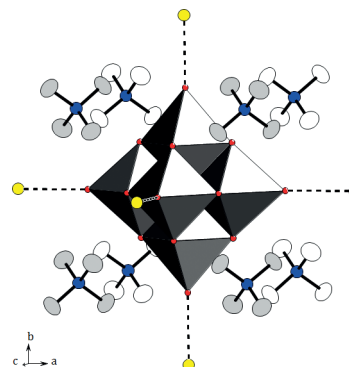


Figure 4. Interactions between the isopolyanionic units and the counter-cations K⁺ and N(CH₃)₄⁺.

The Figure 5 shows a projection of the crystal structure along [101] with evidences of infinite columns of HPA. A general formula can be proposed – TMA₂K[NbW₅O₁₉], which confirms the formation of the expected HPA NbW₅O₁₉³⁻ and shows also that the salt is a mixture of

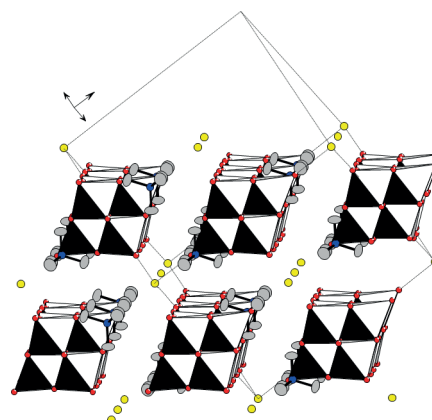


Figure 5. Arrangement of isopolyanions in line along the [101] direction.

TMA and potassium cations, the potassium coming from the $K_8[Nb_6O_{19}]$ niobium precursor.

Furthermore, an XRD diagram was calculated from crystal structure parameters and was compared with an experimental XRD diagram obtained for powder material (Figure 6). It is clearly noticed that both diagrams are identical (with one additional peak for the bulk compound at about 17.5 °C corresponding to traces of physisorbed water or impurities) which leads to the conclusion that even for bulk compound the structure is identical to the one defined for single crystal. This observation confirms that the synthesis is quantitative and the whole powder obtained corresponds to $TMA_2K[NbW_5O_{19}]$, a mixed TMA and potassium salt. The presence of potassium and/or sodium, coming from niobium $K_8[Nb_6O_{19}]$ and tungsten $Na_2WO_4 \cdot 2H_2O$ precursors has already been reported by Dabbabi and Boyer^[35] and Kaezer-França et al.^[36] during the formation of Lindqvist isopolyanion cesium or TMA salts.

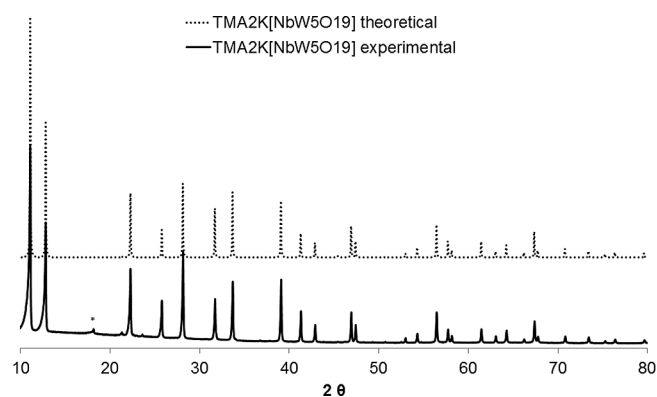


Figure 6. Comparison of theoretical and experimental X-ray pattern for $TMA_2K[NbW_5O_{19}]$.

Thermogravimetric Analysis and Differential Scanning Calorimetry

Thermal stability of synthesized bulk compounds was evaluated by thermogravimetric analysis (TGA). TG curves are reported for potassium salts of $[Nb_6O_{19}]^{8-}$ and $[Nb_4W_2O_{19}]^{6-}$, TMA-potassium mixed salts of $[Nb_xW_{6-x}O_{19}]^{(2+x)-}$ ($x = 3, 2, 1$) and $(NH_4)_6H_2W_{12}O_{40}$ (used for the preparation of reference catalysts) on Figure 7, Figure 8, and Figure 9. Respective DSC analyses were also carried out, results obtained for $(NH_4)_6H_2W_{12}O_{40}$, $[NbW_5O_{19}]^{3-}$ and $[Nb_3W_3O_{19}]^{5-}$ salts are presented.

For $(NH_4)_6H_2W_{12}O_{40}$, its weight loss is followed under nitrogen (Figure 7), its decomposition can be described by the following equation:



The TGA curve shows three weight losses corresponding to loss of water molecules and/or ammonia, characterized by endothermic peaks in DSC (the third one being certainly incorporated into the exothermic peak). Assuming the initial compound formula $(NH_4)_6H_2W_{12}O_{40} \cdot 4H_2O$, first loss of 2.3% corresponds to the release of 4 water molecules whereas the second weight loss (4.6%) is attributed to 6

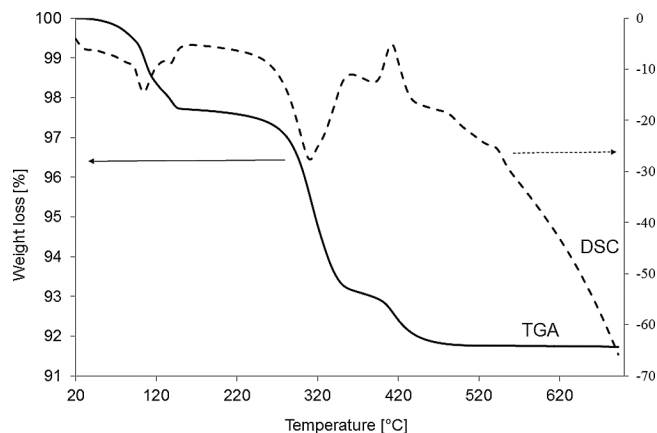


Figure 7. TGA (solid line) and DSC (dashed line) for ammonium metatungstate.

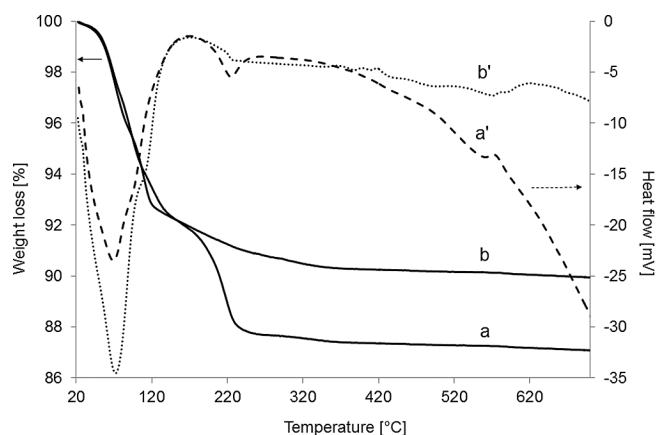


Figure 8. TGA (solid lines) and DSC (dashed lines) curves for $K_8[Nb_6O_{19}]$ (a and a') and $K_6[Nb_4W_2O_{19}]$ (b and b').

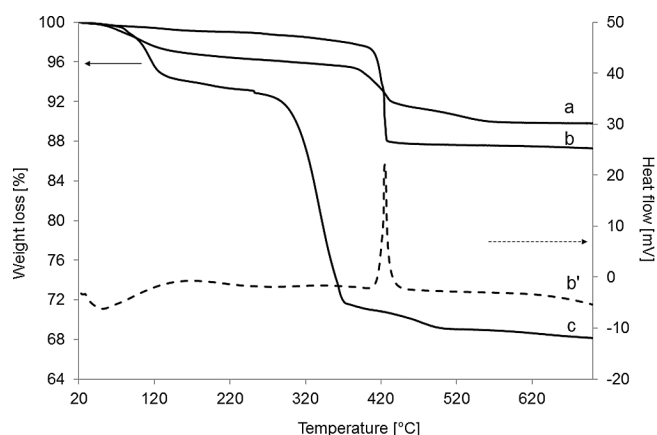


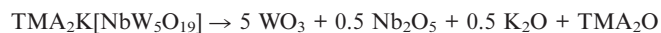
Figure 9. TGA (continuous lines) curves of of TMA salts of $[Nb_xW_{6-x}O_{19}]^{(2+x)-}$ isopolyanions: (a) $TMA_4[Nb_2W_4O_{19}]$ (b) $TMA_2K[NbW_5O_{19}]$ (c) $TMA_5[Nb_3W_3O_{19}]$. DSC of $TMA_2K[NbW_5O_{19}]$ (dashed line b').

ammonia molecules and 2 water molecules. After removal of 6 ammonia and 6 water molecules, at 340 °C a plateau is reached and corresponds to the formation of hydrated oxide $WO_3 \cdot 2H_2O$. Two remaining water molecules are elim-

inated after 380 °C as indicated by the last weight loss observed in TG curve. Simultaneously, crystallization of tungsten trioxide WO₃ is represented by the exothermic peak in the DSC curve. The same range of temperature for WO₃ crystallization was also reported by Marashi et al.^[37] for paratungstate thermal decomposition.

From Figure 8 displaying the thermogravimetric profile of [Nb₆O₁₉]⁸⁻ potassium salt, up to 220 °C we observed the removal of crystalline water from the structure of the hydrated K₈[Nb₆O₁₉] \cdot *n*H₂O. After 220 °C a plateau is reached. Assuming the formation at high temperature of the separated oxides Nb₂O₅ and K₂O, this total water loss of 12.3%, confirmed by two endothermic peaks at 80 and 210 °C, occurs in two continuous steps corresponding to the release of 9 water molecules. The TGA curve of [Nb₄W₂O₁₉]⁶⁻ potassium salt shows a continuous weight loss until 350 °C. This weight loss is very important until 100 °C and is correlated with an endothermic peak observed in DSC curve. From the total weight loss of 9.7%, assuming the formation of Nb₂O₅, WO₃ and K₂O, the number of water molecules is evaluated to 7 indicating the initial salt formulation K₆Nb₄W₂O₁₉ \cdot 7H₂O. It is noted that no exothermic peak corresponding to WO₃ crystallization is shown by DSC curve.

The TGA curves of TMA-potassium mixed salts are reported in Figure 9. In the case of TMA₂K[NbW₅O₁₉]³⁻ which formulae has been determined by XRD measurement, a slight first weight loss correlated to the endothermic peak of the DSC curve is attributed to water loss. Assuming the formation of WO₃, Nb₂O₅ and K₂O this weight loss (1.7%) is attributed to the loss of 1 molecule of H₂O. Between 400 °C and 420 °C, an important weight loss is observed and correlated with an exothermic peak in the DSC curve. The exothermicity is explained by the combustion of TMA that formally corresponds to the loss of (TMA₂O) according to the following equation:



The corresponding weight loss (10.6%) is in agreement with the theoretical weight loss (10.8%) confirming clearly the complete formula TMA₂K[NbW₅O₁₉] \cdot 1H₂O.

For [Nb₂W₄O₁₉]⁴⁻ salt, the weight loss occurs in several steps. The first step is related to water removal, after that a continuous weight loss is observed in two steps: a first one between 380 and 440 °C and a second one with a slower rate between 440 and 560 °C. This total continuous weight loss (6.1%) is too small for explaining the removal of four molecules of TMA and formally corresponds to the weight loss of 2 TMA₂O. Taking into account the presence of potassium in this compound as shown for [NbW₅O₁₉]³⁻ salt, this weight loss is then attributed to the release of 0.25 TMA₂O. In this case, the first weight loss (4%) is due to the loss of 3 water molecules and proposed formula would be TMA_{0.5}K_{3.5}[Nb₂W₄O₁₉] \cdot 3H₂O.

The TGA curve corresponding to the [Nb₃W₃O₁₉]⁵⁻ salt shows also three weight losses. In the same way as for [Nb₂W₄O₁₉]⁴⁻ salt, the first weight loss (6.8%) is attributed to the release of 5 molecules of water, whereas the two con-

tinuous weight losses could be due to the removal of 2 TMA molecules indicating the presence of potassium in this salt for which the proposed formulae is TMA₂K₃[Nb₃W₃O₁₉] \cdot 5H₂O.

Calculations based on weight losses obtained from TGA results allowed us to estimate the release of water and TMA molecules. This estimate lets proposing general formulas and hydration degree of the NbW salts which are presented in Table 1.

Table 1. General formulae based on TGA calculations for NbW compounds.

	General formula
[Nb ₆ O ₁₉] ⁸⁻	K ₈ [Nb ₆ O ₁₉] \cdot 9H ₂ O
[Nb ₄ W ₂ O ₁₉] ⁶⁻	K ₆ [Nb ₄ W ₂ O ₁₉] \cdot 7H ₂ O
[Nb ₃ W ₃ O ₁₉] ⁵⁻	TMA ₂ K ₃ [Nb ₃ W ₃ O ₁₉] \cdot 5H ₂ O
[Nb ₂ W ₄ O ₁₉] ⁴⁻	TMA _{0.5} [K _{3.5} Nb ₂ W ₄ O ₁₉] \cdot 3H ₂ O
[NbW ₅ O ₁₉] ³⁻	TMA ₂ K[NbW ₅ O ₁₉] \cdot 1H ₂ O

It is observed that with increasing niobium content, the hydration degree increases, from 1 for [NbW₅O₁₉]³⁻ till 9 for [Nb₆O₁₉]⁸⁻ isopolyanion. Niobium-based solutions are known to be easily hydrolyzed and this behavior seems in relation to niobium affinity for water molecules.

Solubility

Order of magnitude of solubility values in water at room temperature (r.t.) and at 70 °C for isopolyanions is given in Table 2. The solubility was measured by addition of known water volume (ca. 10 mL in the case of Nb₃W₃O₁₉ salt) to known compound quantity (typically 0.200 g) until complete dissolution of the last compound grain under agitation.

Table 2. Solubility values for [Nb_{6-x}W_xO₁₉]^{(2+x)-} HPA salts.

	Solubility, W [molL ⁻¹] Nb [molL ⁻¹]		
[NbW ₅ O ₁₉] ³⁻	room temp.	2.0 × 10 ⁻³	4.0 × 10 ⁻⁴
	70 °C	4.0 × 10 ⁻³	8.0 × 10 ⁻⁴
[Nb ₂ W ₄ O ₁₉] ⁴⁻	r.t.	5.0 × 10 ⁻³	2.5 × 10 ⁻³
	70 °C	0.02	0.01
[Nb ₃ W ₃ O ₁₉] ⁵⁻	r.t.	0.05	0.05
	70 °C	0.1	0.1
[Nb ₄ W ₂ O ₁₉] ⁶⁻	r.t.	0.07	0.14
	70 °C	0.15	0.3

One can easily notice that those compounds have a very low solubility, even when increasing the temperature. [Nb₄W₂O₁₉]⁶⁻ potassium salt and [Nb₃W₃O₁₉]⁵⁻ mixed TMA-K salt are the most soluble ones. Thus, they were chosen for preparation of the isopolyanions-based catalysts. The solubility of isopolyanions was also verified in other solvents such as ethanol, DMSO, DMF, acetonitrile but water appeared to be the best solvent even if the solubility remains low. Infrared spectra of NbW water solutions showed species preservation after dissolution.

Characterization of Oxide Catalysts

Due to low solubility of synthesized isopoly compounds, only the two most soluble ones were selected for catalysts preparation: $[\text{Nb}_3\text{W}_3\text{O}_{19}]^{5-}$ TMA-K salt and $[\text{Nb}_4\text{W}_2\text{O}_{19}]^{6-}$ potassium salt. Despite their solubility remaining low, WO_3 loading on prepared catalysts was set on 8 wt.-%. The presence of a promoter as nickel is required to form NiWS active HDS phase during sulfidation procedure. In our case nickel was introduced using nickel nitrate solution during a second impregnation step as described in the experimental section to obtain a Ni/W ratio of 0.3 for the catalysts. All the catalysts were characterized in oxidic form by Raman spectroscopy in dried or calcined form.

Raman Spectroscopy

The catalysts in oxidic form were characterized by Raman spectroscopy. Figure 10 shows the Raman spectra of $\text{Nb}_4\text{W}_2\text{Ni}$ and $\text{Nb}_3\text{W}_3\text{Ni}$ catalysts in the dried and calcined state. For all spectra, observed peaks are large. First, for dried samples (Figure 10, b and d), few bands are observed, at about 946 (970) cm^{-1} and 878 (885) cm^{-1} and also at 271 (269) cm^{-1} . The latter well-defined peak corresponding to $\nu_s\text{MO}_c$ vibration suggests that the isopolyanion is preserved after impregnation, maturation and drying. For calcined catalysts, only bands at high wavenumber are observed indicating that isopolyanionic structure is not preserved after calcination at 450 °C. These bands correspond both to polytungstate and polyniobate phases.

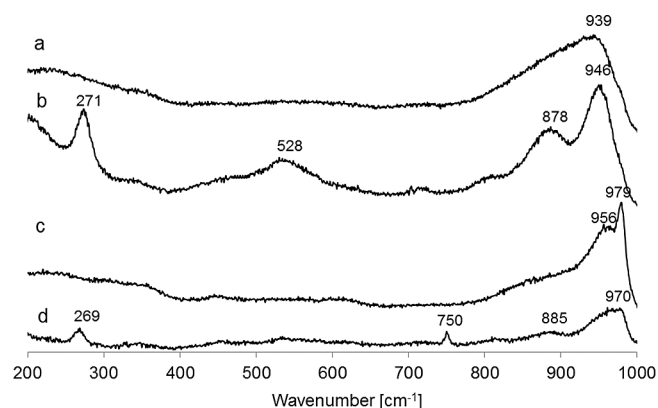


Figure 10. Raman spectra for (a) $\text{Nb}_4\text{W}_2\text{Ni}$ C (b) $\text{Nb}_4\text{W}_2\text{Ni}$ D (c) $\text{Nb}_3\text{W}_3\text{Ni}$ C (d) $\text{Nb}_3\text{W}_3\text{Ni}$ D, where C: calcined catalysts, D: dried catalysts.

Electron Probe Micro Analysis

Figure 11 shows EPMA results allowing the observation of active elements (W, Ni and Nb when present) dispersion in the support extrudate for $\text{Nb}_3\text{W}_3\text{Ni}$ calcined catalyst and for a reference catalyst prepared from conventional precursors (same W and Ni/W ratio). Each image represents a trilobal alumina extrudate in cross section (around 1.5 mm) of calcined catalysts. The elements concentration is represented by color coding – blue representing the lowest concentration, green and yellow for increasing concentration, reaching red color for the highest element loading. For the

isopolyanion-based catalyst the dispersion is homogeneous throughout the interior of the extrudate whatever the element, while for the reference catalyst, heterogeneous dispersion of Ni and W is observed throughout the extrudate. For the isopolyanion-based catalyst niobium and tungsten are introduced in one molecular entity and it can be considered that the heteropolyanionic precursor use is beneficial for homogeneous elements dispersion.

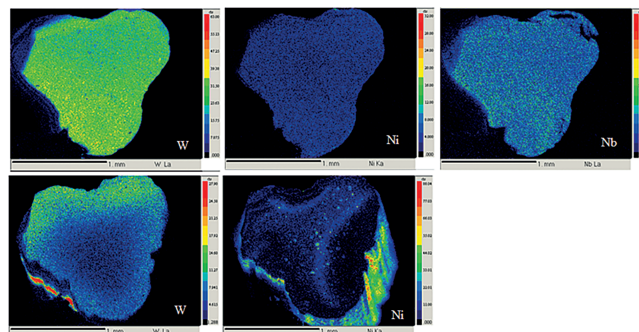


Figure 11. EMPA results for $\text{Nb}_3\text{W}_3\text{Ni}$ C and reference catalysts.

Cyclohexane Isomerization

The isomerization activity of the niobium-containing HPA-based catalysts was evaluated in cyclohexane (CC6) isomerization to give methylcyclopentane on sulfide catalysts under hydrodesulfurization conditions (hydrogen pressure and sulfur presence). The performance of these solids was compared to that of a reference NiW catalyst without niobium (same W and Ni/W ratio). Figure 12 shows that Nb-containing catalysts exhibit higher isomerization activity than the Nb-free catalyst, in particular the $\text{Nb}_3\text{W}_3\text{Ni}$ catalyst that appears 5 times more active than the reference. A slight increase in CC6 conversion is observed in the calcined catalysts when comparing with the performance of the dried solids. $\text{Nb}_4\text{W}_2\text{Ni}$ is less active than $\text{Nb}_3\text{W}_3\text{Ni}$ despite its higher quantity of niobium, it can be related to the presence of a larger quantity of potassium issued from the use of the initial potassium salt $\text{K}_6\text{Nb}_4\text{W}_2$ for preparing $\text{Nb}_4\text{W}_2\text{Ni}$ catalyst.

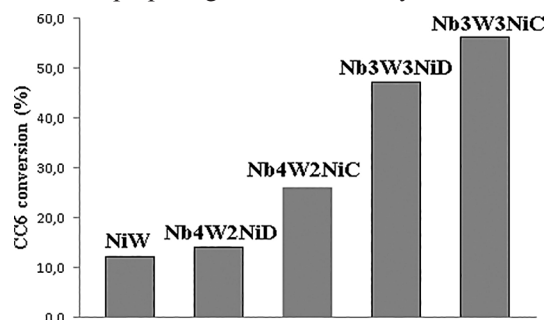


Figure 12. Isomerization conversion for Nb_3W_3 and Nb_4W_2 catalysts (D: dried and C: calcined) compared with NiW catalyst performance. Reaction conditions: 350 °C - hydrogen pressure (60 bars)- feed composition: 4 wt.-% of sulfur, 20.0 wt.-% of toluene and 74.1 wt.-% of cyclohexane.

XPS results (not presented here) have shown that in the studied catalysts niobium entities were unsulfided after the

applied sulfidation procedure (350 °C during 2 h) and present only an oxidic environment. Brønsted acid sites are reported to be involved in cyclohexane isomerization to methylcyclopentane.^[38] We can assume that the polyoxoniobate phase supported on alumina observed by Raman spectroscopy possesses hydroxy groups developing Brønsted acidity requested for CC6 isomerization.

Conclusions

This study focused on the base of Nb-containing Lindqvist isopolyanions $[\text{Nb}_x\text{W}_{6-x}\text{O}_{19}]^{(2+x)-}$. By varying synthesis parameters such as Nb/W ratio, pH or temperature, isopolyanions with $x = 0-4$ and 6 were prepared. The Raman and IR results clearly showed formation of desired compounds. $[\text{NbW}_5\text{O}_{19}]^{3-}$ salt was obtained as a single crystal, X-ray Diffraction and crystallographic study were performed in order to specify the structure of this compound. The XRD theoretical pattern was determined and compared with an experimental one. Those two patterns being identical, one can conclude that the determined structure corresponds not only to single crystal but is also applicable to the bulk material. TGA-based calculations let proposing general formulas; all compounds contain alkaline element and the hydration degree increases with increasing niobium content. The solubility of synthesized compounds was evaluated in several solvents and water appeared to be the best one, even though the solubility remained low. This parameter was a decisive one during selection of materials for catalysts preparation. The two most soluble compounds – $[\text{Nb}_4\text{W}_2\text{O}_{19}]^{6-}$ potassium salt and $[\text{Nb}_3\text{W}_3\text{O}_{19}]^{5-}$ TMA-K salt – were selected to prepare catalysts promoted with nickel (Ni/W = 0.3), that were tested in cyclohexane isomerization after sulfidation. Catalyst prepared from $[\text{Nb}_3\text{W}_3\text{O}_{19}]^{5-}$ TMA-K salt was 5 times more active than a free niobium reference catalyst showing that the presence of niobium in hydrodesulfurization catalysts generates Brønsted acidic sites involved in isomerization reaction, that is recognized for helping HDS of refractory sulfur-containing molecules.

Experimental Section

Isopolyanions Synthesis: $[\text{Nb}_x\text{W}_{6-x}\text{O}_{19}]^{(2+x)-}$ Lindqvist-type isopolyanions were prepared following a protocol of Dabbabi and Boyer^[35] after modifications. In all syntheses, potassium hexaniobate $\text{K}_8[\text{Nb}_6\text{O}_{19}]$, prepared by alkaline fusion of potassium hydroxide (0.98 mol) and niobium oxide (0.05 mol), was used as starting compound. An example of synthesis of potassium and tetramethylammonium (TMA) salts are given below:

$\text{K}_6[\text{Nb}_4\text{W}_2\text{O}_{19}]$: 4×10^{-3} mol of $\text{K}_8[\text{Nb}_6\text{O}_{19}]$ was dissolved in 150 mL of distilled water with addition of 6 mL of hydrogen peroxide. The solution was heated at 60 °C and sodium tungstate dihydrate ($\text{Na}_2\text{WO}_4 \cdot 2\text{H}_2\text{O}$) dissolved in 50 mL of distilled water was then added. The solution was kept at 60 °C under vigorous stirring until complete dissolution of reactants. Then, the solution was acidified with 8 mL of 6 M hydrochloric acid, kept boiling for 10 min and then cooled down to 60 °C. 25 mL of 2 M sodium

hydrogenosulfite was added and the pH was adjusted to 8 with 6 M hydrochloric acid. The solution was placed at 0 °C overnight. Needle-shape crystals of final product were dried under vacuum.

$[\text{Nb}_3\text{W}_3\text{O}_{19}]$ TMA-K Mixed Salt: Tetramethylammonium bromide $[(\text{CH}_3)_4\text{N}]\text{Br}$ (≈ 227 mol) was added to the filtrate after separation of $\text{K}_6[\text{Nb}_4\text{W}_2\text{O}_{19}]$ needles from synthesis described above until complete precipitation of $[\text{Nb}_3\text{W}_3\text{O}_{19}]^{5-}$ salt.

All other $[\text{Nb}_x\text{W}_{6-x}\text{O}_{19}]^{(2+x)-}$ salts were synthesized by modifying above described syntheses parameters such as Nb/W ratio, pH and temperature. The general method of preparation consists in acidification of the solution of sodium tungstate and potassium hexaniobate with set Nb/W ratios, syntheses being performed under heating. In the group of studied compounds, the higher the pH of preparation, the lower content of tungsten is reached. Thus, $[\text{NbW}_5\text{O}_{19}]^{3-}$ is prepared at pH 2.0 and $[\text{Nb}_2\text{W}_4\text{O}_{19}]^{4-}$ at pH 5–6. Stability zones of $[\text{Nb}_2\text{W}_4\text{O}_{19}]^{4-}$, $[\text{Nb}_3\text{W}_3\text{O}_{19}]^{5-}$ and $[\text{Nb}_4\text{W}_2\text{O}_{19}]^{6-}$ niobotungstates are overlaid, making their preparation and separation fragile. The separation of these compounds is based primarily on differences in solubility.

Sodium tungstate dihydrate and niobium oxide were purchased from Sigma and Aldrich and all other reactants used during synthesis from Fisher Scientific.

Catalysts Preparation: The niobium–tungsten catalysts, promoted with nickel, are obtained by sulfidation of oxidic precursors obtained by incipient wetness impregnation of alumina with impregnating solutions based on heteropoly compounds or conventional precursors as described in the following paragraph.

Preparation of the Impregnating Solutions: Impregnating solutions were prepared according to the following procedure:

- Conventional impregnation solution was prepared by dissolution of ammonium metatungstate (AMT).
- Isopolyanions-based impregnation solutions were obtained by isopolyanion salt dissolution in water.
- Solution of nickel precursor was obtained by nickel nitrate dissolution in water, the Ni/W ratio being set on 0.3.

Preparation of the Oxidic Precursors: The oxidic precursors were prepared by incipient wetness impregnation of alumina extrudates (specific area: $265 \text{ m}^2 \text{ g}^{-1}$, total pore volume: 0.75 mL g^{-1}) with previous impregnating solutions. After impregnation and 2 h of maturation in a humid atmosphere in order to allow the species diffusion, the solids were dried for 8 h at 90 °C, nickel was introduced by post-impregnation of the nickel nitrate solution and then the solids were calcined at 450 °C under air. Isopolyanion-based catalysts were prepared in four impregnations due to low precursors solubility. Every impregnation was performed after a drying step. Table 3 resumes prepared catalysts, used precursors and nomenclature. Dried catalysts are noted by a symbol D and calcined ones by symbol C. Following the same procedure Calcined NiW reference catalyst is prepared from ammonium metatungstate (AMT) solution and nickel nitrate solution impregnations after intermediate

Table 3. Prepared catalysts, used precursors and nomenclature.

Catalysts	Precursors	State
Nb3W3NiD	$\text{Nb}_3\text{W}_3\text{O}_{19}$ salt, $\text{Ni}(\text{NO}_3)_2$	dried
Nb3W3NiC	$\text{Nb}_3\text{W}_3\text{O}_{19}$ salt, $\text{Ni}(\text{NO}_3)_2$	calcined
Nb4W2NiD	$\text{Nb}_4\text{W}_2\text{O}_{19}$ salt, $\text{Ni}(\text{NO}_3)_2$	dried
Nb4W2NiC	$\text{Nb}_4\text{W}_2\text{O}_{19}$ salt, $\text{Ni}(\text{NO}_3)_2$	calcined
NiW	AMT, $\text{Ni}(\text{NO}_3)_2$	calcined

Table 4. Crystal data, data collection and structure refinement parameters for single crystal of TMA₂K[NbW₅O₁₉].

Crystal symmetry	cubic
Space group	<i>Fm</i> $\bar{3}$ <i>m</i> (no. 225)
Unit cell [Å]	<i>a</i> = 13.8203(1)
Volume [Å ³]	2639.69(3)
Formula	C ₈ H ₂₄ N ₂ K ₁ Nb ₁ W ₅ O ₁₉
<i>Z</i>	4
<i>M_w</i> , calculated density	1503.5, 3.78205
<i>F</i> (000)	2574
Data collection	
Equipment	Bruker X8
Radiation Mo- <i>K</i> _α [Å]	0.71069
Scan mode	ω/φ-scan
Recorded angular range θ [°]	2.55–32.47
Recording reciprocal space	−20 ≤ <i>h</i> ≤ 20; −18 ≤ <i>k</i> ≤ 20; −20 ≤ <i>l</i> ≤ 20
Number of measured reflections	16393
Number of independent reflections	291
Number of independent reflections [<i>I</i> > 3σ(<i>I</i>)]	271
μ [mm ^{−1}] (λ = Mo- <i>K</i> _α)	22.358
Absorption correction	Semiempirical (Sadabs)
<i>R</i> merging factor [%]	3.60
Refinement parameters	
Software, refinement type	Jana 2000, least squares on <i>F</i>
Number of refined parameters	18
<i>R</i> ₁ (<i>F</i>) all, [<i>I</i> > 3σ(<i>I</i>)] = Σ <i>F</i> _o − <i>F</i> _c /Σ <i>F</i> _o [%]	2.14, 2.05
<i>wR</i> (<i>F</i>) all, [<i>I</i> > 3σ(<i>I</i>)] = [Σ <i>w</i> (<i>F</i> _o − <i>F</i> _c) ² /Σ <i>w</i> (<i>F</i> _o) ²] ^{1/2} [%]	2.50, 2.50
Weight	1/σ ²
Isotropic secondary extinction	Gaussian, 0.083 (8)
Max./min. Δρ [e/Å ³]	1.47/−1.50

drying. WO₃ loading was set on 8 wt.-% and Ni/W ratio on 0.3 for all catalysts.

Precursors and Catalysts Characterization: All compounds were characterized using several techniques. Raman and Infrared spectroscopy confirmed the structure of obtained compounds. Resistance to heating and decomposition under high temperature was determined by thermogravimetric analysis. Finally, for [NbW₅O₁₉]^{3−} anion obtained as single crystal, the structure was determined by XRD and crystallographic study.

Raman Spectroscopy: The Raman spectra of the samples maintained at room temperature were recorded using a Raman microprobe equipped with a photodiode array detector. The exciting laser source was the 532 nm line of a Nd-YAG laser. The wave-number accuracy was 4 cm^{−1}.

Infrared Spectroscopy: Spectra were recorded using a Nicolet 510 Fourier Transform IR spectrometer. The samples were analyzed in the 400–4000 cm^{−1} spectral range using the KBr pellet technique with 1 wt.-% of the sample in KBr. In this work we present spectra in the range 400–1100 cm^{−1} where characteristic tungsten and niobium bands are present.

Single-Crystal and Powder X-ray Diffraction (XRD): A single crystal suitable for X-ray diffraction was isolated from the bulk and mounted on a glass fiber. The data collection was performed using a Bruker X8 diffractometer equipped with an Apex 4k CCD detector. The absorption corrections were performed using the semi-empirical method implanted in SADABS.^[39] Crystal structure was solved using the direct method with SHELXS^[40] and refined using JANA2000.^[41] Data for the data collection and structure refinement are listed in the Table 4.

The homogeneity of the grown single crystals was confirmed by powder XRD after crushing a significant amount of crystals using a D8-Bruker diffractometer with a Cu-*K*_α radiation. The theoretical

diffractogram was calculated from the single-crystal refined model using Powder-cell.^[42]

Thermogravimetric Analysis: The TGA/differential scanning calorimetry experiments were carried out on a Universal V2.6D thermoanalyzer from TA Instruments. The analyses were carried out in air flow, with a heating rate of 10 °C/min and the temperature was raised till 700 °C.

Cyclohexane (CC6) Isomerization in the Presence of Sulfur: CC6 Isomerization activity can be evaluated in the presence of sulfur with dried or calcined catalysts sulfided in situ by dimethyl disulfide (DMDS) added to the charge. In the catalytic test temperature range DMDS is totally decomposed into CH₄ and H₂S. The feed is composed of 5.9 wt.-% of DMDS (giving 4 wt.-% of sulfur), 20.0 wt.-% of toluene and 74.1 wt.-% of cyclohexane. The test is performed in gas phase at a pressure of 60 bars in fixed bed reactor. The procedure is composed of sulfidation followed by catalytic test. The first step takes place from room temperature to 350 °C with temperature increase of 2 °C min^{−1}, GHSV = 4 h^{−1} and H₂/HC ratio = 450NL L^{−1}. The catalytic test is carried out at 350 °C with GHSV = 1 h^{−1} and the same H₂/HC ratio as during the sulfidation step. The isomerization product methylcyclopentane and the cyclohexane reactant are analyzed by gas chromatography. After sulfidation, analysis of effluent through on-line gas chromatography every 2 h after the first measurement was performed. A Scheme (S1) showing all catalytic events is included in supporting information.

Acknowledgments

The authors would like to acknowledge Olivier Delpoux from IFP Energies Nouvelles for his kind and helpful technical assistance and expertise in Raman spectroscopy of catalysts and Nathalie Lett from IFP Energies Nouvelles for catalytic tests.

- [1] N. Mizuno, M. Misono, *Curr. Opin. Solid State Mater. Sci.* **1997**, *2*, 84–89.
- [2] C. I. Cabello, L. L. Botto, H. J. Thomas, *Appl. Catal. A* **2000**, *197*, 79–86.
- [3] A. Griboval, P. Blanchard, L. Gengembre, E. Payen, M. Fournier, J. L. Dubois, J. R. Bernard, *J. Catal.* **1999**, *188*, 102–110.
- [4] D.-L. Long, R. Tsunashima, L. Cronin, *Angew. Chem. Int. Ed.* **2010**, *49*, 1736–1758; *Angew. Chem.* **2010**, *122*, 1780.
- [5] C. Lamonier, C. Martin, J. Mazurelle, V. Harlé, V. D. Guillaume, E. Payen, *Appl. Catal. B* **2007**, *70*, 548–556.
- [6] L. Lizama, T. Klimova, *Appl. Catal. B* **2008**, *82*, 139–150.
- [7] I. V. Kozhevnikov, *Heterogeneous Catalysis by Heteropoly Compound; Polyoxometalate Molecular Science*, Springer, The Netherlands, **2003**, vol. 98, p. 351–380.
- [8] I. V. Kozhevnikov, *Chem. Rev.* **1998**, *98*, 171–198.
- [9] R. D. Shannon, *Acta Crystallogr., Sect. A* **1976**, *32*, 751–767.
- [10] M. T. Pope, *Heteropoly and isopoly oxometalates*, Springer, Berlin, **1983**.
- [11] F. Bannani, H. Driss, R. Thouvenot, M. Debbabi, *J. Chem. Crystallogr.* **2007**, *37*, 37–48.
- [12] J. R. Black, M. Nyman, W. H. Casey, *J. Am. Chem. Soc.* **2006**, *128*, 14712–14720.
- [13] J. Fuchs, W. Freiwald, H. Hartl, *Acta Crystallogr., Sect. B* **1978**, *34*, 1764–1770.
- [14] M. Ziolk, *Catal. Today* **2003**, *78*, 47–64.
- [15] J. Mazurelle, C. Lamonier, C. Lancelot, E. Payen, C. Pichon, D. Guillaume, *Catal. Today* **2008**, *130*, 41–49.
- [16] K. Ben Tayeb, C. Lamonier, C. Lancelot, M. Fournier, E. Payen, A. Bonduelle, F. Bertoncini, *Catal. Today* **2010**, *150*, 207–212.
- [17] K. Ben Tayeb, C. Lamonier, C. Lancelot, M. Fournier, A. Bonduelle-Skrzypczak, F. Bertoncini, *Appl. Catal. B* **2012**, *126*, 55–63.
- [18] P. A. Nikulshin, D. I. Ishutenko, A. A. Mozhaev, K. I. Maslakov, A. A. Pimerzin, *J. Catal.* **2014**, *312*, 152–169.
- [19] S. D. S. Murti, H. Yang, K.-H. Choi, Y. Korai, I. Mochida, *Appl. Catal. A* **2003**, *252*, 331–346.
- [20] T. Isoda, S. Nagao, X. Ma, Y. Korai, I. Mochida, *Energy Fuels* **1996**, *10*, 1078–1082.
- [21] J. Marques, D. Guillaume, I. Merdrignac, D. Espinat, S. Brunet, *Appl. Catal. B* **2011**, *101*, 727–737.
- [22] A. Omegna, J. A. van Bokhoven, R. Prins, *J. Phys. Chem. B* **2003**, *107*, 8854–8860.
- [23] T. C. Ho, A. R. Katritzky, S. J. Cato, *Ind. Eng. Chem. Res.* **1992**, *31*, 1589–1597.
- [24] M. Hino, M. Kurashige, H. Matsushashi, K. Arata, *Appl. Catal. A* **2006**, *310*, 190–193.
- [25] K. Okumura, K. Yamashita, K. Yamada, M. Niwa, *J. Catal.* **2007**, *245*, 75–83.
- [26] K. Tanabe, S. Okazaki, *Appl. Catal. A* **1995**, *133*, 191–218.
- [27] R. Bértolo, A. Martins, J. M. Silva, F. Ribeiro, A. Fernandes, *Microporous Mesoporous Mater.* **2011**, *143*, 284–290.
- [28] C. Geantet, J. Afonso, M. Breyse, N. Allali, M. Danot, *Catal. Today* **1996**, *28*, 23–30.
- [29] N. Allali, E. Prouzet, A. Michalowicz, V. Gaborit, A. Nadiri, M. Danot, *Appl. Catal. A* **1997**, *159*, 333–354.
- [30] S. Bej, S. K. Maity, U. T. Turaga, *Energy Fuels* **2004**, *18*, 1227–1237.
- [31] C. Rocchiccioli-Deltcheff, R. Thouvenot, M. Dabbabi, *Spectrochim. Acta Part A* **1977**, *33*, 143–153.
- [32] C. Rocchiccioli-Deltcheff, M. Fournier, R. Franck, R. Thouvenot, *Inorg. Chem.* **1983**, *22*, 207–216.
- [33] M. Mylrajan, *J. Mol. Struct.* **1995**, *348*, 233–236.
- [34] M. Mylrajan, *J. Chem. Phys.* **1988**, *89*, 1634.
- [35] M. Dabbabi, M. Boyer, *J. Inorg. Nucl. Chem.* **1976**, *38*, 1011–1014.
- [36] M. C. Kaezer França, J.-G. Eon, M. Fournier, E. Payen, O. Mentré, *Solid State Sci.* **2005**, *7*, 1533–1541.
- [37] M. S. Marashi, J. Vahdati Khaki, S. M. Zebarjad, *Int. J. Refractory Metals Hard Materials* **2012**, *30*, 177–179.
- [38] J. Abbot, *J. Catal.* **1990**, *123*, 383–395.
- [39] G. M. Sheldrick, *SADABS: Area Detector Absorption Correction*, Madison, WI, USA, **1996**.
- [40] G. M. Sheldrick, *SHELXTL package* - Bruker Analytical X-ray Systems, Madison, WI, USA, **1997**.
- [41] G. M. Sheldrick, V. Petricek, M. Dusek, *The crystallographic computing system JANA2000*, Institute of Physics, Prague, Czech Republic, **2000**.
- [42] W. Krauss, G. Nolze, *Powder-cell*, v. 2.4, Federal Institute for Materials Research and Testing, Rudower Chaussee 5, Berlin.

Received: December 3, 2014
Published Online: March 13, 2015